Inorganic Chemistry

Communication

Cite This: Inorg. Chem. 2017, 56, 12682-12686

pubs.acs.org/IC

Electronic Conductivity in a Porous Vanadyl Prussian Blue Analogue upon Air Exposure

Mary Anne Manumpil,[†] Carmen Leal-Cervantes,[†] Matthew R. Hudson,[‡] Craig M. Brown,[‡] and Hemamala I. Karunadasa*[,†]

[†]Department of Chemistry, Stanford University, Stanford, California 94305, United States

[‡]Center for Neutron Research, National Institute of Standards and Technology, Gaithersburg, Maryland 20899, United States

Supporting Information

ABSTRACT: Exposure to humid O_2 or ambient air affords a 5-order-of-magnitude increase in electronic conductivity of a new Prussian blue analogue incorporating Co^{II} and V^{IV}-oxo units. Oxidation produces a mixed-valence framework, where the O_2 exposure time controls the V^{IV}/V^{V} ratio and thereby the material's conductivity. The oxidized framework shows an intervalence charge-transfer band at ca. 4200 cm^{-1}, consistent with mixed valence. The mixed-valence frameworks show semiconducting behavior with conductivity values of 10^{-5} S·cm^{-1} at room temperature and 10^{-4} S·cm^{-1} at 100 °C and activation energies of ca. 0.3 eV. N_2 adsorption measurements at 77 K show that these materials possess permanent porosity before and after oxidation with Brunauer–Emmett–Teller surface areas of 340 and 370 $m^2 \cdot g^{-1}$, respectively.

Prussian blue analogues (PBAs) are a versatile class of coordination compounds with corner-sharing metal cyanide octahedra, which form an open three-dimensional framework.[1] Here, cyanide-mediated electronic interactions between metal centers give rise to a multitude of magnetic[2,3] electrical,[4] and electrochromic[5] phenomena. Owing to their porosity, these frameworks can also capture and store small molecules such as O_2, H_2, CO_2, and SO_2.[6−8] Although the electrical properties of the original Prussian blue (PB) framework ($Fe_4[Fe(CN)_6]_3$) have been well studied,[9−18] only a handful of electrically conductive PBAs have been reported to date (Table S3).[4,17−21] Even rarer are reports of electrically conductive and porous PBAs.[17] PB is a porous semiconductor with room-temperature conductivity values ranging from 10^{-11} to 10^{-5} S·cm^{-1} with increasing water and interstitial ion content.[11,12,16,17] Dehydrated PB, with no interstitial ions, has a Brunauer–Emmett–Teller (BET) surface area of 550 $m^2 \cdot g^{-1}$[22] and conductivity values of 10^{-7}–10^{-11} S·cm^{-1}.[12,15,16] Inclusion of heavier metals with more diffuse orbitals has afforded a higher conductivity of 5.7×10^{-3} S·cm^{-1} at 300 K in the PBA $K_{1.2}Ru_{3.6}[Ru(CN)_6]_3$, which has a BET surface area of 325 $m^2 \cdot g^{-1}$.[17]

Here we report a large increase in conductivity upon air exposure in a new porous PBA featuring vanadium oxo units with the approximate formula $Co[VO(CN)_4]$ (**1**). Although most PBAs feature hexacyanometallates, metal centers with less than six cyanides also form these frameworks.[23−25] For example, air oxidation of V^{II} or V^{III} centers in V–Cr PBAs[26−29] and electrochemical reduction of the V^{V} sites in V–Fe PBAs[30,31] have previously afforded vanadyl groups in these frameworks, diagnosed by characteristic V≡O stretches in their vibrational spectra. Prior to this work, we were not aware of PBAs formed through the solution-state self-assembly of vanadyl units.

Framework **1** was synthesized by combining stoichiometric aqueous solutions of $(VO)SO_4$, $Co(NO_3)_2$, and KCN under N_2 to yield a fine brown hydrated powder (Figure S1). Inductively coupled plasma atomic emission spectroscopy (ICP-AES) showed that the V:Co ratio in **1** is close to 1:1 and that the K content is negligible (see the Supporting Information). As is the case with many cyanide-containing PBAs,[26,28,29,32,33] reliable analyses for C and N from combustion could not be obtained. Using ICP-AES analysis for the metal content, combustion analysis for the water content, and charge balance to deduce the CN content gives the formula for **1** as $K_aCo_b[VO(CN)_c]\cdot dH_2O$, where a = 0.03–0.05, b = 0.88–0.93, c = 3.80–3.92, d = 0.53–1.67, with small compositional variations between batches (Table S1). Slight changes in synthetic conditions are known to change the stoichiometry of PBAs because of the rapid, irreversible precipitation of these highly insoluble frameworks.[20,33,34] We also synthesized the vanadyl-zinc PBA, where the formula was similarly determined to be $K_{0.043}Zn_{0.69}[VO(CN)_{3.42}]\cdot 0.69H_2O$ (**2**).

Similar to most PBAs,[35,36] **1** does not form crystals suitable for single-crystal X-ray diffraction. Rietveld refinement of powder X-ray diffraction (PXRD) data, however, reveals a PBA structure with space group $Fm\bar{3}m$ and a lattice parameter of 10.1949(1) Å (Figure 1). Oxo ligands were placed in the model because they could not be distinguished from the cyanide ligands owing to their similar electron densities. Each cyanide (fixed at $^4/_6$ occupancy per site) and each oxo (fixed at $^1/_6$ occupancy per site) are equally disordered over six sites to preserve the lattice's cubic symmetry (see the Supporting Information). Upon dehydration, **1** becomes very dark blue and partially retains its crystallinity (Figure S3).

The vibrational spectrum of **1** features a band at 2175 cm^{-1}, indicative of bridging cyanides.[37] We assign the band at 976 cm^{-1} to the terminal V≡O stretch (Figure S4).[38] A similar band at 981 cm^{-1} has been reported in $(VO)[Cr(CN)_6]_{2/3}$.[27] When **1** is synthesized in $H_2{}^{18}O$, this band is shifted to 933 cm^{-1} (Figure S5). This 43 cm^{-1} shift agrees well with the shift of 42 cm^{-1}

Received: August 10, 2017
Published: October 23, 2017

DOI: 10.1021/acs.inorgchem.7b02051
Inorg. Chem. 2017, 56, 12682–12686

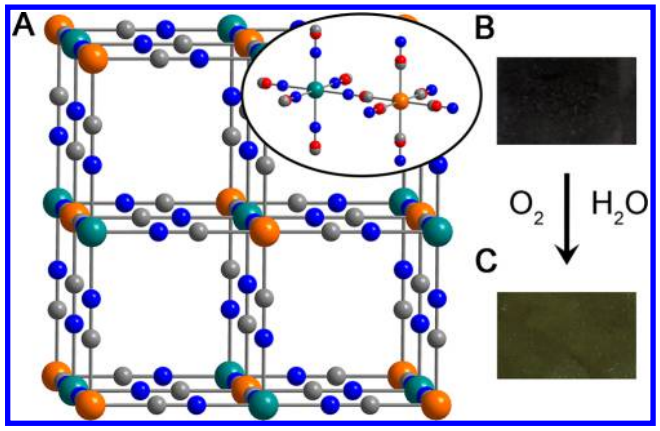

Figure 1. (A) Structure of **1** obtained by Rietveld refinement of PXRD data. Interstitial water molecules and disordered oxo ligands are omitted for clarity. Orange, teal, gray, and blue spheres represent V, Co, C, and N atoms, respectively. Inset: Metal coordination environment with disordered oxo ligands (red). Dehydrated powders of **1** change from dark blue (B) to green (C) upon oxidation.

predicted from the harmonic oscillator model, confirming the incorporation of vanadyl units in **1**.

The solid-state electron paramagnetic resonance (EPR) spectrum of **1** (Figure 2) reveals a broad peak with a *g* value of

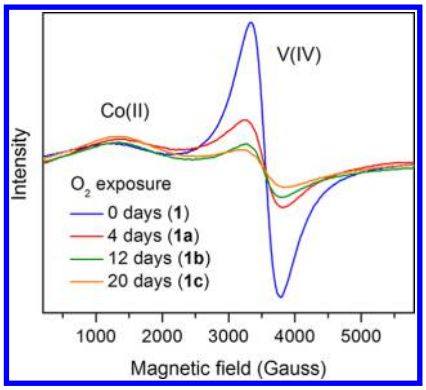

Figure 2. EPR spectra of **1** upon exposure to water-saturated O_2 for 4 (**1a**), 12 (**1b**), and 20 (**1c**) days.

ca. 3.6, which is assigned to high-spin Co^{II} octahedrally coordinated to the N ends of the cyanides. We see a similar band in the EPR spectrum of $Co_3[Co(CN)_6]_2$, which contains paramagnetic high-spin Co^{II} and diamagnetic low-spin Co^{III} centers (Figure S6). Furthermore, the $g \sim 3.6$ feature is absent in the spectrum of the VO−Zn PBA **2** (Figure S7), corroborating that it originates from the Co^{II} centers in **1**. The V^{IV} signal in **1** appears as a broad isotropic peak with a *g* value of 1.94, which is similar to values reported for molecular vanadyl centers.[39] We do not see the hyperfine interaction that is typically observed for a V^{IV} nucleus in **1**. This may be due to the high concentration of V^{IV} centers that causes dipolar spin−spin coupling, which broadens the EPR signal.[40,41] Additionally, the EPR spectrum of the VO−Zn PBA **2** contains only a broad peak with a *g* value of 1.94 (Figure S7), similar to that seen in **1**, corroborating its assignment to the V.

Solid **1** reacts with air under ambient conditions to form a dark-green framework, with a fraction of the V^{IV} centers oxidized to V^{V}. To perform more controlled oxidation, we exposed powders of **1** to a flow of water-saturated O_2 gas to obtain the mixed-valence framework **1a**. No detectable oxidation occurs when **1** powders are exposed to dry O_2 gas over 7 days, suggesting that water is required for the oxidation. Our efforts to identify possible charge-balancing ions that must enter/leave the framework upon oxidation have been impeded by the lack of spectroscopic signatures in **1a**, as discussed below (Figures S4 and S8). Indeed, postsynthetically oxidized V-containing PBAs have only been characterized by their vanadyl stretches using vibrational spectroscopy.[2,26−29,32]

Oxidation does not produce detectable changes in the material's PXRD pattern (Figure S9). Upon oxidation, the vanadyl stretch shifts from 976 to 993 cm^{-1} (Figure S4). Because the d_{xy}-based highest occupied molecular orbital of the vanadyl center in a tetragonal ligand field[39] has primarily nonbonding character with respect to the axial oxo ligand, this increased stretching frequency suggests an electrostatically stronger V^{V}−O bond. Except for this change, the mid- and far-IR spectra of **1** and **1a** are very similar (Figures S4 and S8). The solid-state EPR spectrum of **1** shows that the V^{IV} signal's intensity decreases upon oxidation, indicating the formation of EPR-silent V^{V} sites (Figure 2).

Using EPR spin quantification (see the Supporting Information) and ICP-AES, we determined the V^{IV}/V^{V} ratio in **1** after oxidation. Although double integration of solid-state EPR data is not always precise,[42] we calculated approximate V^{IV}/V^{V} ratios (Figure S10) using this method. We used powders of **1** as a reference, assuming that all V centers were V^{IV}. Longer exposure time to water-saturated O_2 results in more oxidized materials with lower V^{IV}/V^{V} ratios. Exposure of **1** to an O_2/H_2O flow for 0,

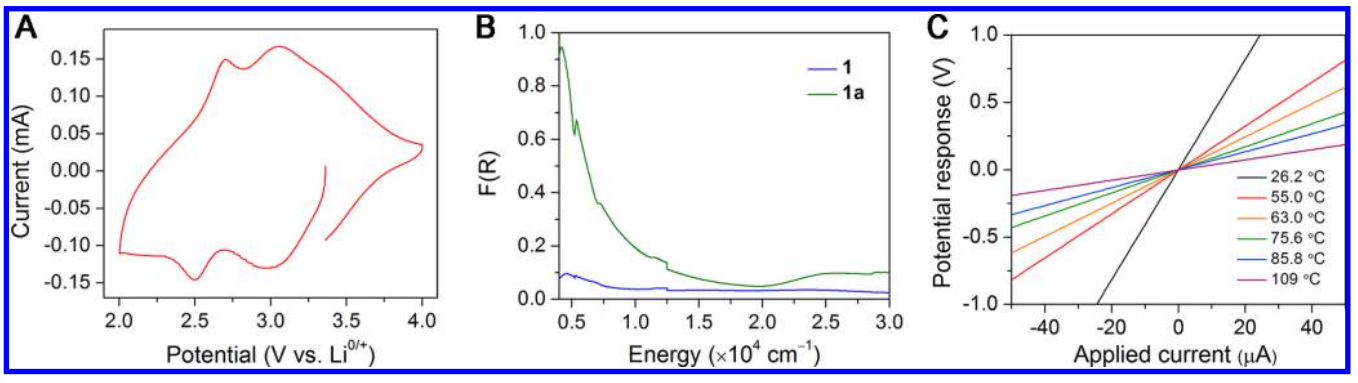

Figure 3. (A) Solid-state CV of **1a**. (B) Diffuse-reflectance UV−vis−NIR spectra of **1** and **1a**. $F(R)$ is the Kubelka−Munk transform of the diffuse-reflectance spectra. (C) Current−voltage curves of **1a**.

DOI: 10.1021/acs.inorgchem.7b02051
Inorg. Chem. 2017, 56, 12682−12686

4, 12, and 20 days resulted in materials with V^{IV}/V^{V} ratios of 1.0:0 (**1**), 2.8:1.0 (**1a**), 0.90:1.0 (**1b**), and 0.87:1.0 (**1c**), respectively.

The solid-state cyclic voltammogram (CV) of **1a** reveals that the V^{IV}/V^{V} redox couple is split into two broad peaks with $E_{1/2}$ values at 3.0 and 2.6 V versus $Li^{+/0}$ (Figure 3A). To eliminate the possibility that these peaks originated from the Co centers, we measured the CV of the oxidized VO−Zn PBA **2a**. The solid-state CV of **2a** shows two broad peaks with $E_{1/2}$ values at 3.1 and 2.6 V versus $Li^{+/0}$ (Figure S11). Because Zn^{II} is not redox-active in the experimental potential range, we assign these peaks to the V^{IV}/V^{V} redox couple. The splitting of peaks and the peak width suggest electronic communication between multiple V centers and are characteristic of mixed-valence materials.[43,44]

The diffuse-reflectance UV−vis−near-IR measurement of **1a** exhibits an absorbance from ca. 19000 to 4000 cm^{-1} (corresponding to our detection limit), which is absent in the spectrum of **1** (Figure 3B). An absorbance from ca. 19000 to 4000 cm^{-1} also appears in the spectrum of **2a** and is absent in that of **2** (Figure S12). We therefore assign these new bands in **1a** and **2a** as vanadyl-based IVCT bands, indicating mixed valence.[45,46] Within our instrumental detection limits, we cannot analyze the IVCT band shape to assign a class[44] for the degree of mixed valence. Because of the disordered ligands in the framework, there could be multiple electronic coupling pathways between vanadyl centers. A molecular V^{IV}/V^{V} mixed-valence polyoxovanadate has a reported IVCT band from 12000 to 4000 cm^{-1}.[47] We do not observe the low-energy tail of the IVCT band in the mid-IR region of the vibrational spectrum, likely because of the bandwidth and the lack of instrument sensitivity.[48]

Because mixed-valence materials can often transport charge,[46] we performed four-point-probe resistivity measurements on pressed pellets of dehydrated **1** and **1a**−**1c** in the van der Pauw configuration.[49] Absorbed water changes the dielectric constant of PB, and its activation energy for conduction (E_a), therefore, decreases with increasing water content.[11,12,16−18] Thus, we performed conductivity measurements under dry N_2 on dehydrated samples of **1a**−**1c**. Current−voltage curves for dehydrated **1** measured at both room temperature and 100 °C show negligible current response, revealing its insulating nature (Figure S13). Based on instrumental detection limits, the upper limit of the conductivity of dehydrated **1** is ca. 10^{-10} $S{\cdot}cm^{-1}$ at room temperature. In contrast, current−voltage curves for the dehydrated frameworks **1a**−**1c** display ohmic behavior characteristic of conductive materials with an increase in conductivity of 5 orders of magnitude. Frameworks **1a**−**1c** behave as semiconductors, consistent with class II mixed-valence materials, with conductivity values increasing from 10^{-5} $S{\cdot}cm^{-1}$ at room temperature up to 10^{-4} $S{\cdot}cm^{-1}$ at 100 °C (Table 1, Figures 3C and S14−S18). Higher V^{V} content yields increased conductivity and lowered E_a values. To probe ionic contribution to the conductivity, we performed impedance measurements on dehydrated pellets of **1a**−**1c** using stainless steel blocking electrodes. The absence of capacitive tails in the impedance plots indicates dominant electronic conductivity in **1a**−**1c** (Figure S19).[50] Charge transport in these mixed-valence materials is believed to occur through thermally activated electron hopping, which is the accepted mechanism for conduction in PBAs.[10,12−21] The E_a values of dehydrated **1a**−**1c** are lower than that reported for dehydrated PB (Table S3).[15] The maximum energy of framework **1a**'s IVCT band is less than 4200 cm^{-1}, which is therefore at least 10000 cm^{-1} lower in energy than that of PB's IVCT band (Figure S20), helping to explain why dehydrated **1a** is more conductive than dehydrated PB.

Table 1. Ratios of V^{IV}/V^{V} Centers, Conductivity Values (σ), and Activation Energies (E_a) of 1 and 1a−1c

	V^{IV}/V^{V} ratio	σ at 298 K ($S{\cdot}cm^{-1}$)	σ at 373 K ($S{\cdot}cm^{-1}$)	E_a (eV)
1	1.0:0	$<10^{-10}$	$<10^{-10}$	N/A
1a	2.8:1	3.4×10^{-5}	3.7×10^{-4}	0.285(3)
1b	0.90:1	6.4×10^{-5}	5.5×10^{-4}	0.276(4)
1c	0.87:1	7.2×10^{-5}	6.2×10^{-4}	0.265(9)

A N_2 isotherm at 77 K reveals permanent porosity in **1** with a BET surface area of 340 $m^2{\cdot}g^{-1}$. Importantly, the conductive framework **1a** maintains porosity upon oxidation with a similar BET surface area of 370 $m^2{\cdot}g^{-1}$ (Figure S21).

In conclusion, we report the postsynthetic oxidation of a new PBA through a solid−gas reaction to yield a porous and electrically conductive framework. Although the conductivity values of **1a**−**1c** are lower than those of the most conductive metal−organic frameworks, these PBAs are robust and scalable. Site isolation of redox-active centers in extended frameworks and their postsynthetic oxidation can lead to sorbents for small-molecule capture that can be inexpensively regenerated through potential-swing cycles.

■ ASSOCIATED CONTENT

Supporting Information

The Supporting Information is available free of charge on the ACS Publications website at DOI: 10.1021/acs.inorgchem.7b02051.

Experimental details and spectra (PDF)

Accession Codes

CCDC 1559091 contains the supplementary crystallographic data for this paper. These data can be obtained free of charge via www.ccdc.cam.ac.uk/data_request/cif, or by emailing data_request@ccdc.cam.ac.uk, or by contacting The Cambridge Crystallographic Data Centre, 12 Union Road, Cambridge CB2 1EZ, UK; fax: +44 1223 336033.

■ AUTHOR INFORMATION

Corresponding Author

*E-mail: hemamala@stanford.edu.

ORCID

Hemamala I. Karunadasa: 0000-0003-4949-8068

Notes

The authors declare no competing financial interest.

■ ACKNOWLEDGMENTS

This work was supported by a National Science Foundation (NSF) CAREER award (DMR-1351538). M.A.M. thanks the NSF (DGE-114747) and Stanford's Diversifying Academia, Recruiting Excellence Program, for fellowships. PXRD was performed at the Stanford Nano Shared Facilities, supported by the NSF (ECCS-1542152). Synchrotron PXRD was performed at Argonne National Laboratory under the U.S. Department of Energy (DE-AC02-06CH11357). We thank A. Jacobs, S. Jones, Dr. R. Hadt, Dr. M. Aubrey, M. Gonzalez, and Dr. H. R. Lee for helpful discussions, Dr. P. Giraldo and L. Darago for experimental assistance, and Prof. E. I. Solomon for access to equipment.

DOI: 10.1021/acs.inorgchem.7b02051
Inorg. Chem. 2017, 56, 12682−12686

REFERENCES

(1) Keggin, J. F.; Miles, F. D. Structures and Formulæ of the Prussian Blues and Related Compounds. *Nature* **1936**, *137*, 577−578.
(2) Ferlay, S.; Mallah, T.; Ouahès, R.; Veillet, P.; Verdaguer, M. A Room-Temperature Organometallic Magnet Based on Prussian Blue. *Nature* **1995**, *378*, 701−703.
(3) Aguilà, D.; Prado, Y.; Koumousi, E. S.; Mathonière, C.; Clérac, R. Switchable Fe/Co Prussian Blue Networks and Molecular Analogues. *Chem. Soc. Rev.* **2016**, *45*, 203−224.
(4) Sato, O.; Kawakami, T.; Kimura, M.; Hishiya, S.; Kubo, S.; Einaga, Y. Electric-Field-Induced Conductance Switching in FeCo Prussian Blue Analogues. *J. Am. Chem. Soc.* **2004**, *126*, 13176−13177.
(5) Neff, V. D. Electrochemical Oxidation and Reduction of Thin Films of Prussian Blue. *J. Electrochem. Soc.* **1978**, *125*, 886−887.
(6) Kaye, S. S.; Choi, H. J.; Long, J. R. Generation and O_2 Adsorption Studies of the Microporous Magnets $CsNi[Cr(CN)_6]$ (T_C = 75 K) and $Cr_3[Cr(CN)_6]_2\bullet 6H_2O$ (T_N = 219 K). *J. Am. Chem. Soc.* **2008**, *130*, 16921−16925.
(7) Kaye, S. S.; Long, J. R. Hydrogen Storage in the Dehydrated Prussian Blue Analogues $M_3[Co(CN)_6]_2$ (M = Mn, Fe, Co, Ni, Cu, Zn). *J. Am. Chem. Soc.* **2005**, *127*, 6506−6507.
(8) Thallapally, P. K.; Motkuri, R. K.; Fernandez, C. A.; McGrail, B. P.; Behrooz, G. S. Prussian Blue Analogues for CO_2 and SO_2 Capture and Separation Applications. *Inorg. Chem.* **2010**, *49*, 4909−4915.
(9) Inoue, H.; Yanagisawa, S. Bonding Nature and Semiconductivity of Prussian Blue and Related Compounds. *J. Inorg. Nucl. Chem.* **1974**, *36*, 1409−1411.
(10) England, S. J.; Kathirgamanathan, P.; Rosseinsky, D. R. Perturbation Calculation from the Charge-Transfer Spectrum Data of Intervalence Site-Transfer D.C. Conductivity in Prussian Blue. *J. Chem. Soc., Chem. Commun.* **1980**, 840−841.
(11) Ganguli, S.; Bhattacharya, M. Studies of Different Hydrated Forms of Prussian Blue. *J. Chem. Soc., Faraday Trans. 1* **1983**, *79*, 1513−1522.
(12) Tennakone, K.; Dharmaratne, W. G. D. Experimental and Theoretical Study of Electronic Conduction in H_2O-Doped Prussian Blue. *J. Phys. C: Solid State Phys.* **1983**, *16*, 5633−5639.
(13) Feldman, B. J.; Murray, R. W. Electron Diffusion in Wet and Dry Prussian Blue Films on Interdigitated Array Electrodes. *Inorg. Chem.* **1987**, *26*, 1702−1708.
(14) Rosseinsky, D. R.; Tonge, J. S.; Berthelot, J.; Cassidy, J. F. Site-Transfer Conductivity in Solid Iron Hexacyanoferrates by Dielectric Relaxometry, Voltammetry and Spectroscopy. Prussian Blue, Congeners and Mixtures. *J. Chem. Soc., Faraday Trans. 1* **1987**, *83*, 231−243.
(15) Inoue, H.; Nakazawa, T.; Mitsuhashi, T.; Shirai, T.; Fluck, E. Characterization of Prussian Blue and Its Thermal Decomposition Products. *Hyperfine Interact.* **1989**, *46*, 723−731.
(16) Xidis, A.; Neff, V. D. On the Electronic Conduction in Dry Thin Films of Prussian Blue, Prussian Yellow, and Everitt's Salt. *J. Electrochem. Soc.* **1991**, *138*, 3637−3642.
(17) Behera, J. N.; D'Alessandro, D. M.; Soheilnia, N.; Long, J. R. Synthesis and Characterization of Ruthenium and Iron−Ruthenium Prussian Blue Analogues. *Chem. Mater.* **2009**, *21*, 1922−1926.
(18) Pajerowski, D. M.; Watanabe, T.; Yamamoto, T.; Einaga, Y. Electronic Conductivity in Berlin Green and Prussian Blue. *Phys. Rev. B: Condens. Matter Mater. Phys.* **2011**, *83*, 153202.
(19) Yamada, S.; Kuwabara, K.; Koumoto, K. Characterization of Prussian Blue Analogue: Nanocrystalline Nickel−Iron Cyanide. *Mater. Sci. Eng., B* **1997**, *49*, 89−94.
(20) Molnár, G.; Cobo, S.; Mahfoud, T.; Vertelman, E. J. M.; van Koningsbruggen, P. J.; Demont, P.; Bousseksou, A. Interplay between the Charge Transport Phenomena and the Charge-Transfer Phase Transition in $Rb_xMn[Fe(CN)_6]_y\bullet zH_2O$. *J. Phys. Chem. C* **2009**, *113*, 2586−2593.
(21) Tennakone, K. The Activation of N-Type Semiconduction in Ferrocyanides and P-Type Semiconduction in Ferricyanides by Interstitial Water. *J. Phys. C: Solid State Phys.* **1983**, *16*, L1193−L1196.
(22) Kaye, S. S.; Long, J. R. The Role of Vacancies in the Hydrogen Storage Properties of Prussian Blue Analogues. *Catal. Today* **2007**, *120*, 311−316.
(23) Ayers, J. B.; Waggoner, W. H. Synthesis and Properties of a Series of Pentacyanoferrates. *J. Inorg. Nucl. Chem.* **1969**, *31*, 2045−2051.
(24) Fluck, E.; Inoue, H.; Nagao, M.; Yanagisawa, S. Bonding Properties in Prussian Blue Analogues of the Type $Fe[Fe(CN)_5X]\bullet xH_2O$. *J. Inorg. Nucl. Chem.* **1979**, *41*, 287−292.
(25) Beauvais, L. G.; Long, J. R. $Co_3[Co(CN)_5]_2$: A Microporous Magnet with an Ordering Temperature of 38 K. *J. Am. Chem. Soc.* **2002**, *124*, 12096−12097.
(26) Dujardin, E.; Ferlay, S.; Phan, X.; Desplanches, C.; Cartier dit Moulin, C.; Sainctavit, P.; Baudelet, F.; Dartyge, E.; Veillet, P.; Verdaguer, M. Synthesis and Magnetization of New Room-Temperature Molecule-Based Magnets: Effect of Stoichiometry on Local Magnetic Structure by X-Ray Magnetic Circular Dichroism. *J. Am. Chem. Soc.* **1998**, *120*, 11347−11352.
(27) Ferlay, S.; Mallah, T.; Ouahès, R.; Veillet, P.; Verdaguer, M. A Chromium−Vanadyl Ferrimagnetic Molecule-Based Magnet: Structure, Magnetism, and Orbital Interpretation. *Inorg. Chem.* **1999**, *38*, 229−234.
(28) Hatlevik, O.; Buschmann, W. E.; Zhang, J.; Manson, J. L.; Miller, J. S. Enhancement of the Magnetic Ordering Temperature and Air Stability of a Mixed Valent Vanadium Hexacyanochromate (III) Magnet to 99 °C (372 K). *Adv. Mater.* **1999**, *11*, 914−918.
(29) Holmes, S. M.; Girolami, G. S. Sol−Gel Synthesis of $K^{II}V^{III}[Cr^{III}(CN)_6]\bullet 2H_2O$: A Crystalline Molecule-Based Magnet with a Magnetic Ordering Temperature above 100 °C. *J. Am. Chem. Soc.* **1999**, *121*, 5593−5594.
(30) Shaojun, D.; Fengbin, L. Researches on Chemically Modified Electrodes: Part XV. Preparation and Electrochromism of the Vanadium Hexacyanoferrate Film Modified Electrode. *J. Electroanal. Chem. Interfacial Electrochem.* **1986**, *210*, 31−44.
(31) Carpenter, M. K.; Conell, R. S.; Simko, S. J. Electrochemistry and Electrochromism of Vanadium Hexacyanoferrate. *Inorg. Chem.* **1990**, *29*, 845−850.
(32) Garde, R.; Villain, F.; Verdaguer, M. Molecule-Based Room-Temperature Magnets: Catalytic Role of V(III) in the Synthesis of Vanadium−Chromium Prussian Blue Analogues. *J. Am. Chem. Soc.* **2002**, *124*, 10531−10538.
(33) Entley, W. R.; Girolami, G. S. High-Temperature Molecular Magnets Based on Cyanovanadate Building Blocks: Spontaneous Magnetization at 230 K. *Science* **1995**, *268*, 397−400.
(34) Vertelman, E. J. M.; Maccallini, E.; Gournis, D.; Rudolf, P.; Bakas, T.; Luzon, J.; Broer, R.; Pugzlys, A.; Lummen, T. T. A.; van Loosdrecht, P. H. M.; van Koningsbruggen, P. J. The Influence of Defects on the Electron-Transfer and Magnetic Properties of $Rb_x[MnFe(CN)_6]_y\bullet zH_2O$. *Chem. Mater.* **2006**, *18*, 1951−1963.
(35) Verdaguer, M.; Girolami, G. S. Magnetic Prussian Blue Analogs. In *Magnetism: Molecules to Materials V*; Miller, J. S., Drillon, M., Eds.; Wiley-VCH Verlag GmbH & Co. KGaA: Weinheim, Germany, 2005; pp 283−346.
(36) Choudhury, S.; Bagkar, N.; Dey, G. K.; Subramanian, H.; Yakhmi, J. V. Crystallization of Prussian Blue Analogues at the Air−Water Interface Using an Octadecylamine Monolayer as a Template. *Langmuir* **2002**, *18*, 7409−7414.
(37) Nakamoto, K. *Infrared and Raman Spectra of Inorganic and Coordination Compounds Part B: Applications in Coordination, Organometallic, and Bioinorganic Chemistry*, 5th ed.; John Wiley & Sons, Inc.: New York, 1997; pp 105−113.
(38) Selbin, J. The Chemistry of Oxovanadium(IV). *Chem. Rev.* **1965**, *65*, 153−175.
(39) Ballhausen, C. J.; Gray, H. B. The Electronic Structure of the Vanadyl Ion. *Inorg. Chem.* **1962**, *1*, 111−122.
(40) Drago, R. S. *Physical Methods in Chemistry*, 1st ed.; W. B. Saunders: Philadelphia, PA, 1977; pp 348−349.
(41) Ooms, K.; Polenova, T.; Shough, A. M.; Doren, D. J.; Nash, M. J.; Lobo, R. F. Identification of Mixed Valence Vanadium in ETS-10 Using Electron Paramagnetic Resonance, ^{51}V Solid-State Nuclear Magnetic

DOI: 10.1021/acs.inorgchem.7b02051
Inorg. Chem. 2017, 56, 12682−12686

Resonance, and Density Functional Theory Studies. *J. Phys. Chem. C* **2009**, *113*, 10477−10484.
(42) Yordanov, N. D. Quantitative EPR Spectrometry − "State of the Art". *Appl. Magn. Reson.* **1994**, *6*, 241−257.
(43) Creutz, C. Mixed Valence Complexes of d^5−d^6 Metal Centers. In *Progress in Inorganic Chemistry*; Lippard, S. J., Ed.; John Wiley & Sons, Inc.: Hoboken, NJ, 1983; Vol. *30*, pp 1−73.
(44) D'Alessandro, D. M.; Keene, F. R. Current Trends and Future Challenges in the Experimental, Theoretical and Computational Analysis of Intervalence Charge Transfer (IVCT) Transitions. *Chem. Soc. Rev.* **2006**, *35*, 424−440.
(45) D'Alessandro, D. M.; Keene, F. R. A Cautionary Warning on the Use of Electrochemical Measurements to Calculate Comproportionation Constants for Mixed-Valence Compounds. *Dalton Trans.* **2004**, 3950−3954.
(46) Robin, M. B.; Day, P. Mixed Valence Chemistry−A Survey and Classification. *Adv. Inorg. Chem. Radiochem.* **1968**, *10*, 247−422.
(47) Keene, T. D.; D'Alessandro, D. M.; Krämer, K. W.; Price, J. R.; Price, D. J.; Decurtins, S.; Kepert, C. J. $[V_{16}O_{38}(CN)]^{9-}$: A Soluble Mixed-Valence Redox-Active Building Block with Strong Antiferromagnetic Coupling. *Inorg. Chem.* **2012**, *51*, 9192−9199.
(48) Currell, G. *Analytical Instrumentation: Performance Characteristics and Quality*; John Wiley & Sons, Ltd.: Chichester, U.K., 2000; pp 67−89.
(49) Schroder, D. K. *Semiconductor Material and Device Characterization*, 3rd ed.; John Wiley & Sons, Inc.: Hoboken, NJ, 2006; pp 1−20.
(50) Huggins, R. A. *Advanced Batteries: Materials Science Aspects*; Springer Science: New York, 2009; pp 423−430.

DOI: 10.1021/acs.inorgchem.7b02051
Inorg. Chem. 2017, 56, 12682−12686